Supporting information

In Situ Construction of FeCo Alloy Nanoparticles Embedded in Nitrogen-Doped Bamboo-like Carbon Nanotubes as a Bifunctional Electrocatalyst for Zn-Air Battery

Junxue Chen [a, †], Jie Zhu [c], SiJia Li [a], Zhonglin Li [a], Chengzhi Wu [a], Ding Wang [a], Zhihong Luo [a], Yibing Li [a, *], Kun Luo [b, *]

[a] *Key Lab of New Processing Technology for Nonferrous Metal & Materials, Ministry of Education; School of Materials Science and Engineering, Guilin University of Technology, Guilin 541000, P. R. China*

[b] *School of Materials Science and Engineering, Changzhou University, Changzhou 213164, P. R. China*

c School of Chemistry and Chemical Engineering, Beijing Institute of Technology, Beijing 100081, P. R. China

[*] Corresponding Authors: *E-mails*: lybgems@glut.edu.cn (Libing Li), luokun@cczu.edu.cn (Kun Luo)

Characterizations

The crystal structure of the samples was analyzed by X-ray diffraction (XRD, X'Pert PRO) using Cu Kα radiation (λ = 1.5406 Å). Field emission scanning electron microscopy (FESEM) for microstructures was performed using a Hitachi S-4800 instrument operating at a voltage of 5 kV. Transmission electron microscopy (TEM), high-resolution transmission electron microscopy (HRTEM), high-annular dark-field and bright-field scanning transmission electron microscopy (STEM), energy dispersive X-ray spectroscopy (EDS) images were obtained on Transmission Electron Microscope (Titan G2 60-300). Raman spectra were obtained using a Thermo Fisher Scientific DXR with a 532 nm laser. The specific area and pore size distribution of the samples were determined by nitrogen adsorption/desorption isotherm measurements using a Tristar II 3020 gas adsorption analyzer. X-ray photoelectron spectroscopy (XPS) measurement was performed on ESCALAB 250XI spectrometer with Al Kα X-ray radiation as the X-ray source for excitation.

Electrochemical measurements

All electrochemical tests were performed on electrochemical workstation (Chenhua, CHI760E) with a three-electrode system at room temperature. Ring disk electrode (RDE, 5 mm diameter) used as working electrode, a graphite rod as counter electrode, and Hg/HgO as reference electrode. All potential values were given with the respective to reversible hydrogen electrode (RHE) scale and converted from Hg/HgO electrode by using $E_{(RHE)} = E_{(Hg/HgO)} + 0.059\ pH + 0.098$ (25 °C). In this work, 5 mg of catalytic material, 25 μL of Nafion (5 wt%), and 300 μL of absolute ethanol were added into 700 μL of high-purity water, and ultrasound for 30 min to form an evenly dispersed catalyst ink. Then the ink catalyst (4 μL) was dropped onto working electrode with an electrochemical loading of 0.28 mg cm^{-2}, then dried at room temperature. The commercial Pt/C (20 wt%) and IrO_2 were obtained with equivalent mass loadings.

To assess the ORR catalytic activity, cyclic voltammetry (CV) measurements were carried out at a scan rate of 50 mV s^{-1} in an Ar/O_2-saturated 0.1 M KOH solution. Then, linear sweep voltammetry (LSV) profiles were performed with a scan rate of 5 mV s^{-1}

in O_2-saturated 0.1 M KOH solution under different disk rotation rates. The Tafel slope was obtained from the corresponding LSV curve. The ORR stability was assessed by chronoamperometric responses with a rotation rate of 400 rpm in O_2-saturated 0.1 M KOH solution. For the anti-methanol test, the current was recorded when 3.0 M methanol was added into the electrolyte at 300 s.

The electron transfer number (n) and kinetic current density (J_K) for a typical ORR are calculated from the Koutecky-Levich equations:

$$J^{-1} = J_K^{-1} + B^{-1}\omega^{-1} \quad (3)$$

$$B = 0.2nFC_O D_0^{2/3} \nu^{-1/6} \quad (4)$$

Where J and J_K are the measured current density and kinetic current density respectively; ω is the speed of RDE (rpm); v is the dynamic viscosity of the electrolyte (0.01 cm^2 s^{-1} in 0.1 mol L^{-1} KOH solution); F is the Faraday constant (F = 96485 C mol^{-1}); C_O is the concentration of oxygen in the electrochemical reaction (1.2×10^{-3} mol L^{-1} in a 0.1 mol L^{-1} KOH solution), D_O is oxygen diffusion coefficient ($1.93\times10^{-5}cm^2$ s^{-1} in 0.1 mol L^{-1} KOH solution).

In order to further verify the number of transferred electrons, use the following equation to calculate the H_2O_2 yield and the number of transferred electrons:

$$H_2O_2\% = 2\frac{I_r}{I_d + \frac{I_r}{N}} \times 100\% \quad (5)$$

$$n = 4\frac{I_d}{I_d + \frac{I_r}{N}} \quad (6)$$

In which I_r and I_d represent the ring current and the Faradaic current densities at the disc, N is the current collecting efficiency of the Pt ring and determined to be 0.43.

When test the OER catalytic activity, the LSV measurements were carried out in O_2 saturated 1 M KOH solution. All polarization curves were 85%-iR compensation. Electrochemical impedance spectroscopy (EIS) measurements were carried out in the same condition at open-circuit voltage from 1 to 10^5 Hz with a voltage of 5 mV. The electrochemical active surface area (ECSA) was determined by measuring the

capacitive current associated with double-layer charging from the scan-rate dependence of CVs.

Zin-air battery measurements.

The liquid Zn-air battery was fabricated, in which 6.0 M KOH + 0.2 M $Zn(CH_3COO)_2 \cdot 2H_2O$ solution was employed as electrolyte, zinc sheet served as the anode and FeCo/N-CNTs-800-loaded carbon cloth (4 mg cm^{-2}) served as the air cathode, respectively. As the comparation, the battery was also assembled using the mixed catalyst of commercial Pt/C (20 wt%) and IrO_2 with mass ratio of 1:1. All the testing measurements in this work were conducted at room temperature and pressure.

Supplementary Figures

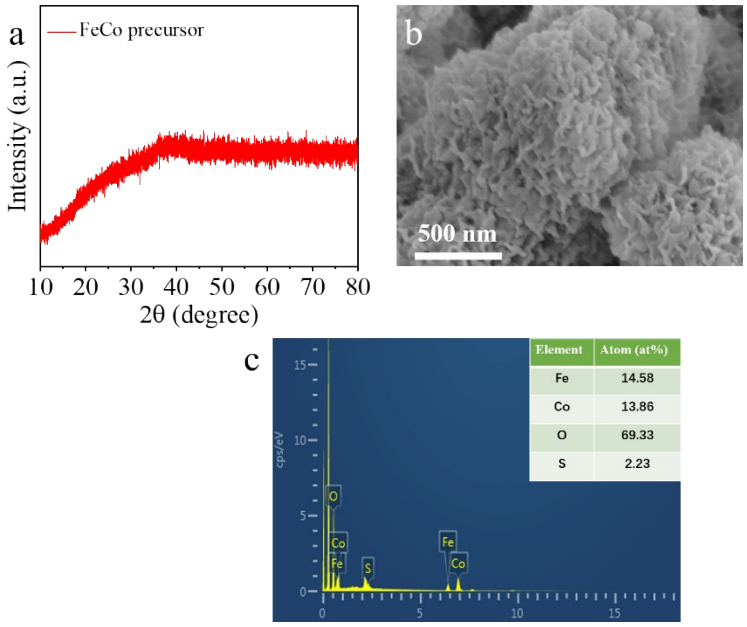

Fig. S1 (a) XRD pattern, (b) FESEM image and (c) EDS analysis of FeCo precursor.

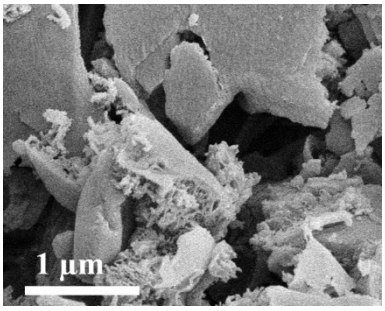

Fig. S2 FESEM of pure CN-550.

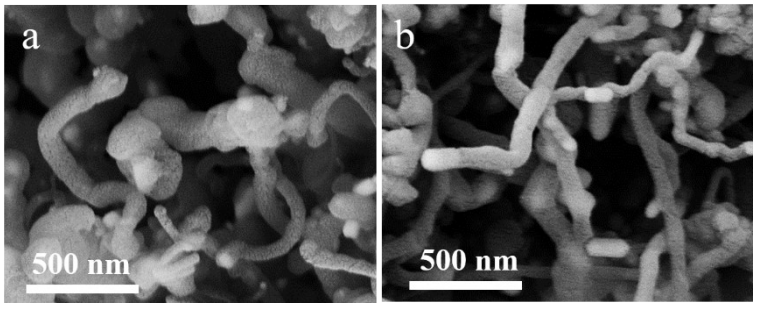

Fig. S3 FESEM images of (a) Co/N-CNTs-800 and (b) Fe/N-CNTs-800 samples.

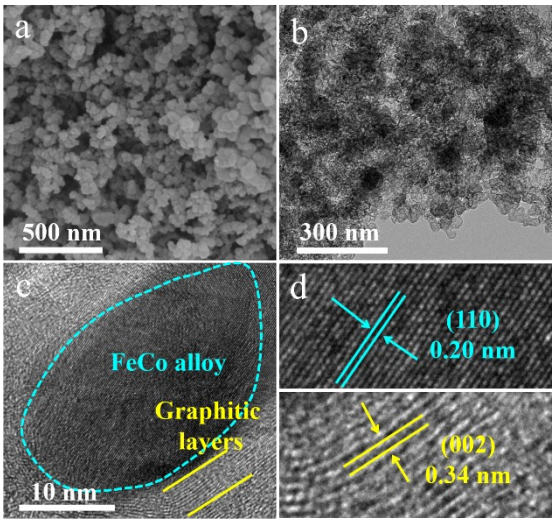

Fig. S4 (a) FESEM, (b) TEM and (c-d) HRTEM images of FeCo/CB-800.

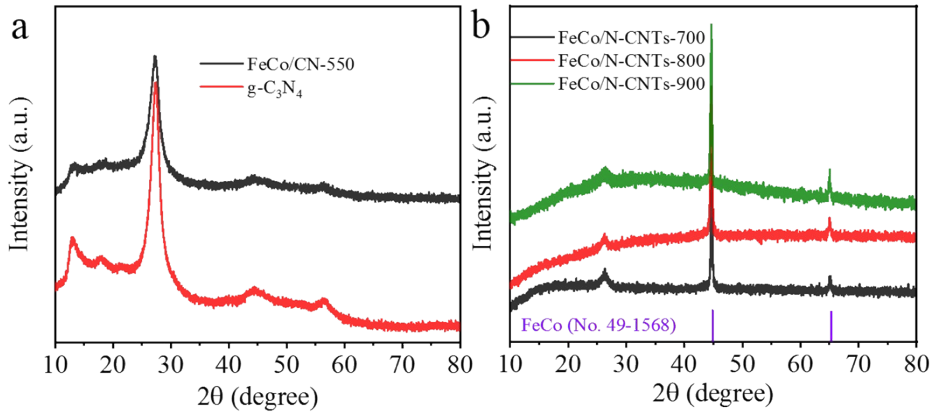

Fig. S5 (a) XRD patterns of FeCo/CN-550 and g-C_3N_4 samples. (b) XRD patterns of FeCo/N-CNTs-700, FeCo/N-CNTs-800 and FeCo/N-CNTs-900 samples.

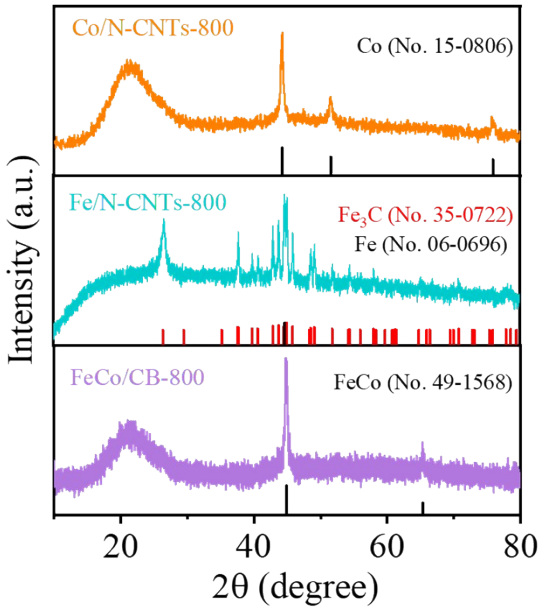

Fig. S6 XRD patterns of Co/N-CNTs-800, Fe/N-CNTs-800 and FeCo/CB-800 samples.

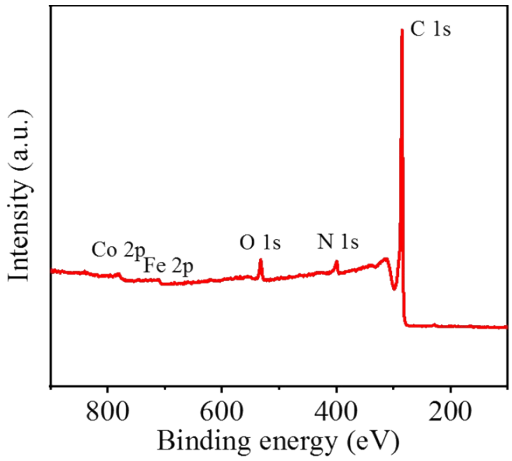

Fig. S7 XPS survey spectrum of FeCo/N-CNTs-800.

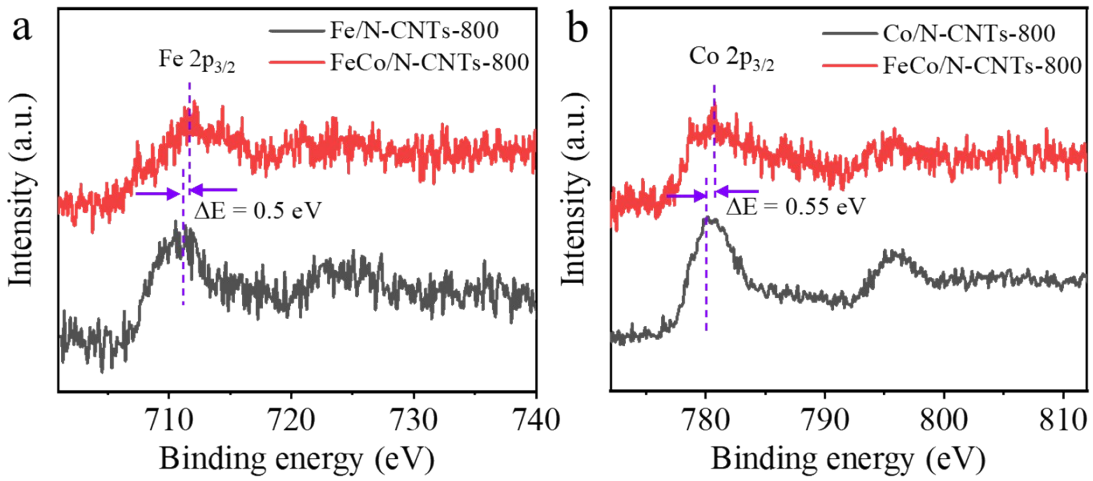

Fig. S8 (a) High-resolution Fe 2p XPS spectra for FeCo/N-CNTs-800 and Fe/N-CNTs-800, (b) high-resolution Co 2p XPS spectra for FeCo/N-CNTs-800 and Co/N-CNTs-800.

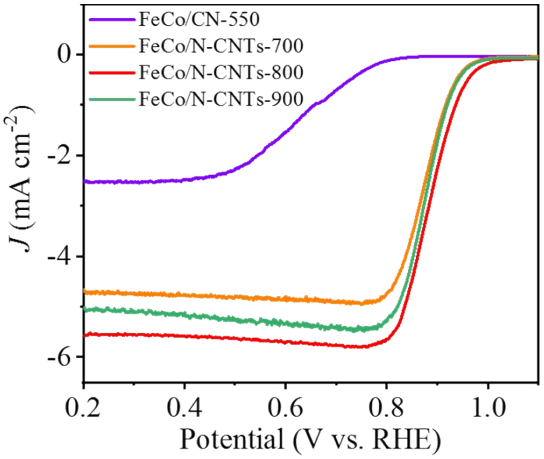

Fig. S9 LSV curves of FeCo/N-CNTs-T catalysts synthesized at different pyrolysis temperatures (550, 700, 800 and 900 °C) in O_2-saturated 0.1 M KOH solution at a rotation speed of 1600 rpm.

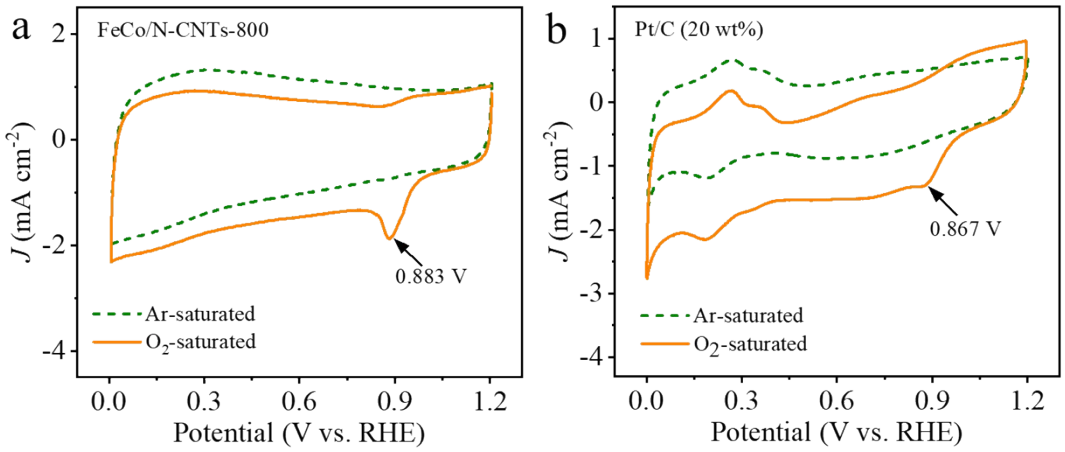

Fig. S10 CVs of (a) FeCo/N-CNTs-800 and (b) Pt/C (20 wt%) in O_2-saturated and Ar-saturated 0.1 M KOH solution at a scan rate of 5 mV s^{-1}.

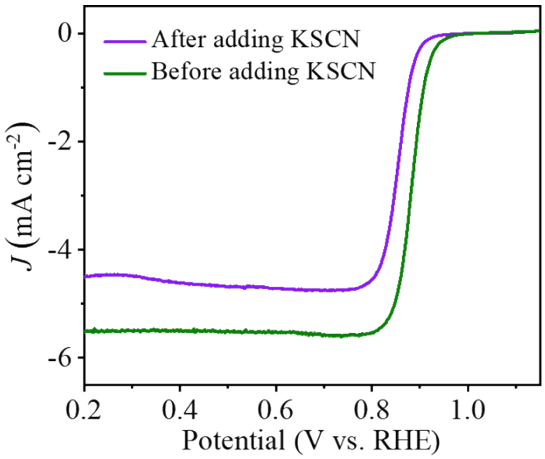

Fig. S11 (a) LSV curves of FeCo/N-CNTs-800 in O_2-saturated 0.1 M KOH before and after the addition of 0.05 M KSCN.

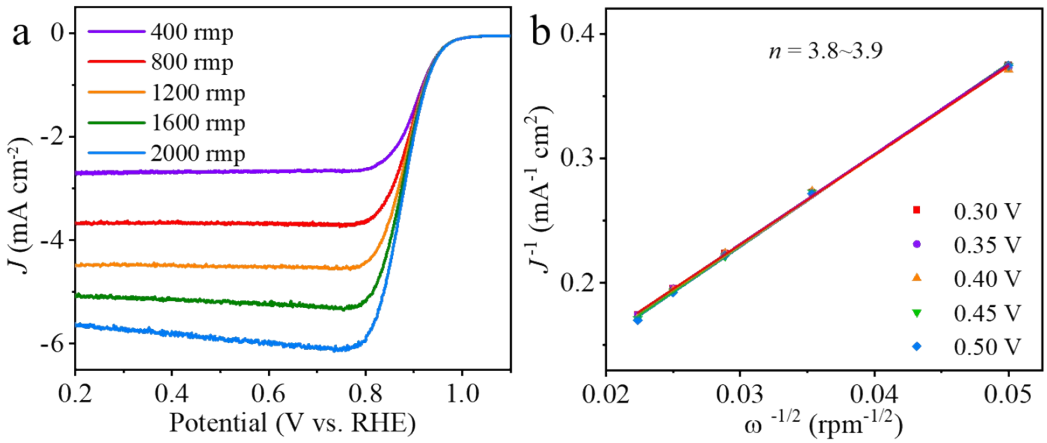

Fig. S12 (a) LSV curves of Pt/C (20 wt%) at different rotation speeds and (b) corresponding Koutecky-Levich plots for Pt/C (20 wt%) at different potentials.

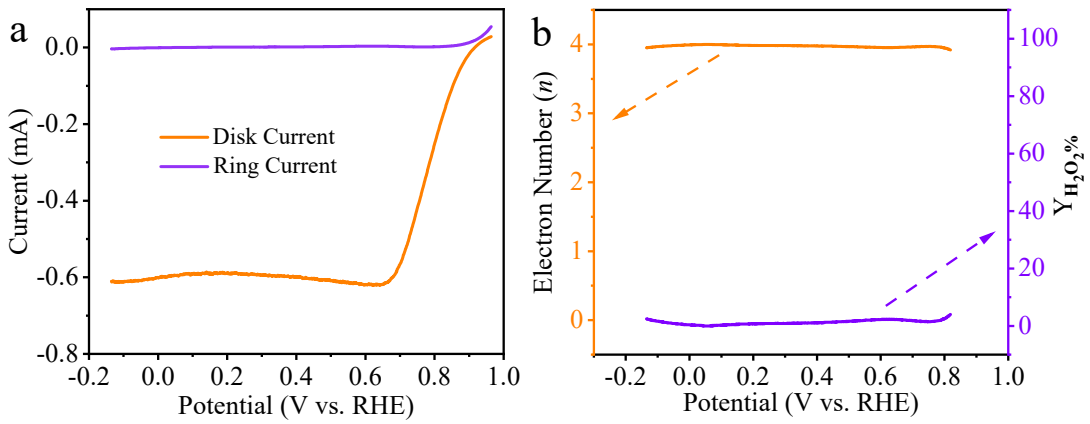

Fig. S13 RRDE polarization curves (a) and the overall electron transfer number and H_2O_2 yield (b) of FeCo/N-CNTs-800.

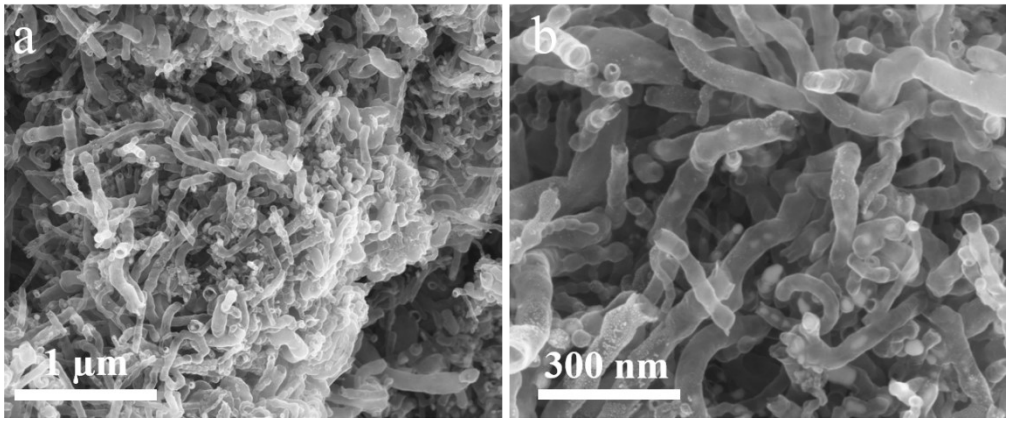

Fig. S14 (a and b) SEM images of the after-ORR FeCo/N-CNTs-800 in 0.1 M KOH.

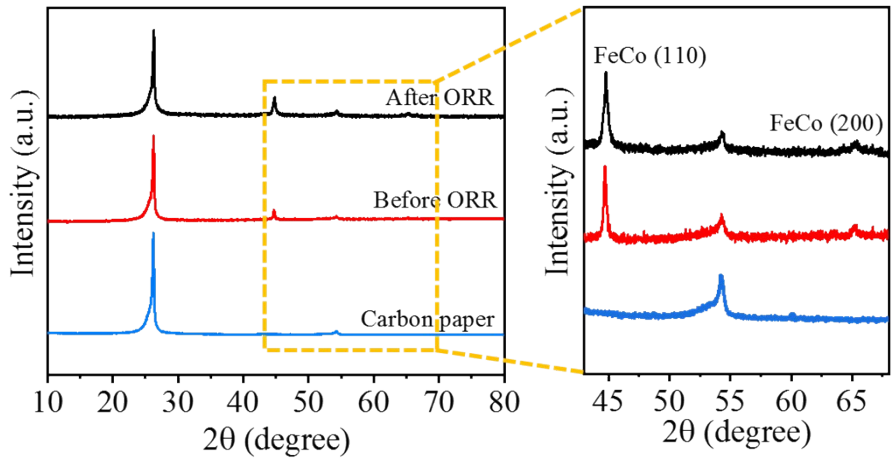

Fig. S15 XRD pattern of FeCo/N-CNTs-800 loaded on carbon paper before and after the ORR reaction in 0.1 M O_2-saturated KOH solution.

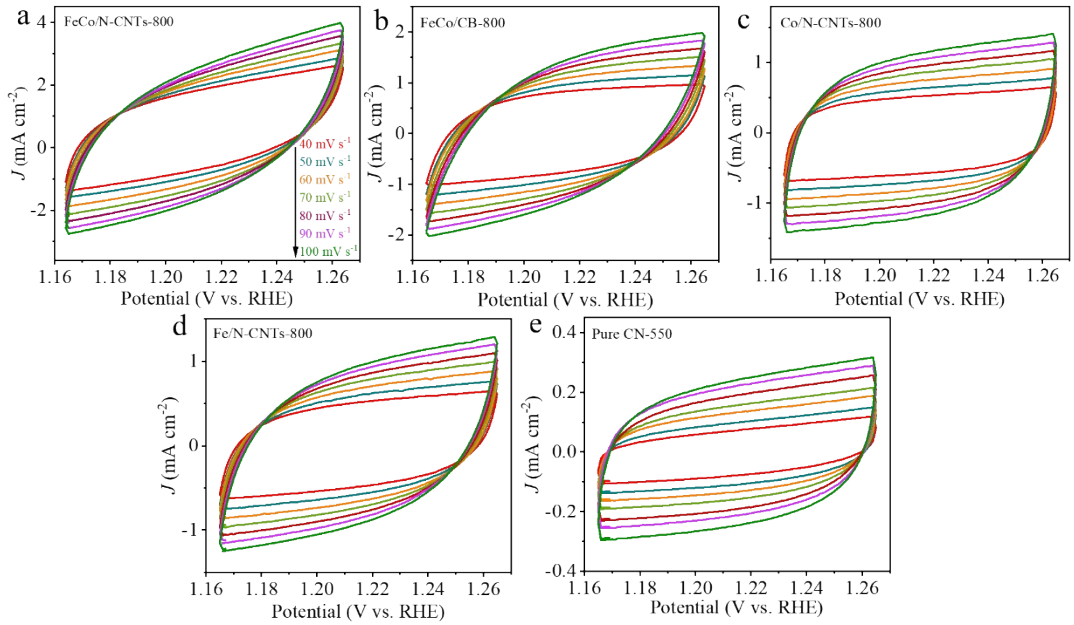

Fig. S16 CV curves of (a) FeCo/N-CNTs-800, (b) FeCo/CB-800, (c) Co/N-CNTs-800, (d) Fe/N-CNTs-800 and (e) pure CN-550 in 1 M KOH with different scan rates.

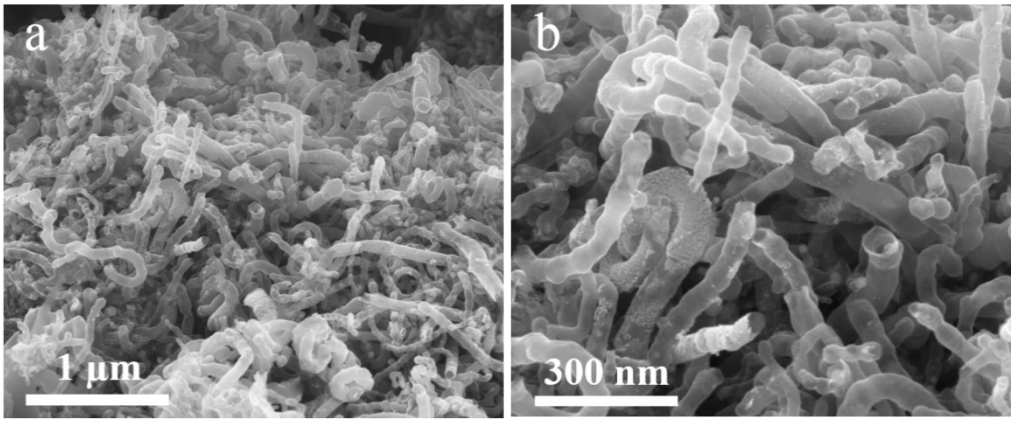

Fig. S17 (a and b) SEM images of the after-OER FeCo/N-CNTs-800 in 1.0 M KOH.

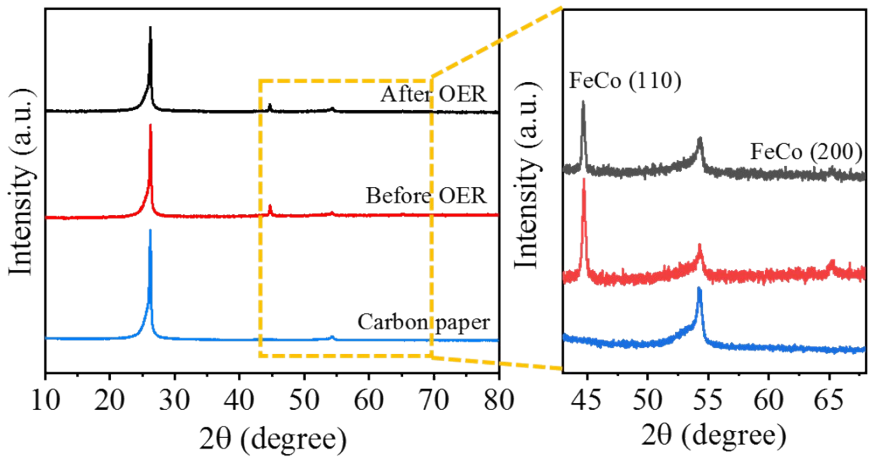

Fig. S18 XRD pattern of FeCo/N-CNTs-800 loaded on carbon paper before and after the OER reaction in 1.0 M KOH solution.

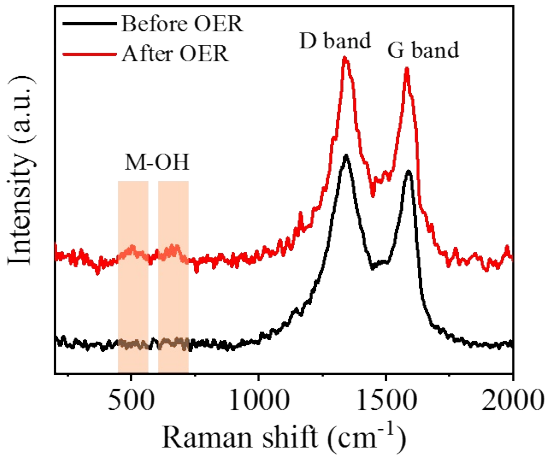

Fig. S19 Raman spectra of FeCo/N-CNTs-800 loaded on carbon paper before and after OER reaction in 1.0 M KOH solution.

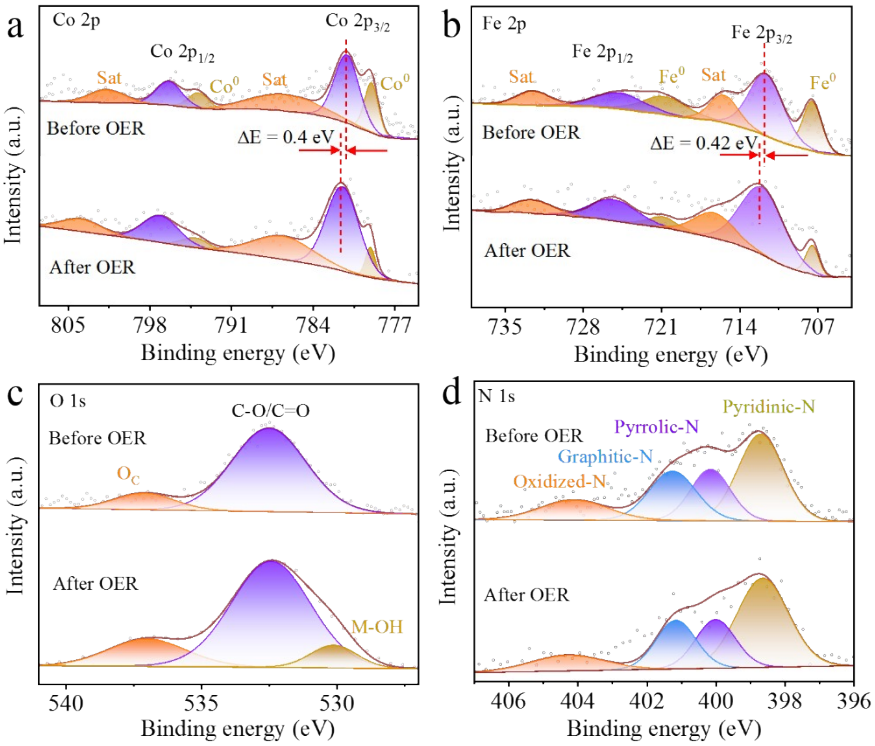

Fig. S20 High-resolution (a) Co 2p, (b) Fe 2p, (c) O 1s and (d) N 1s XPS spectra of FeCo/N-CNTs-800 loaded on carbon paper before and after OER reaction in 1.0 M KOH solution.

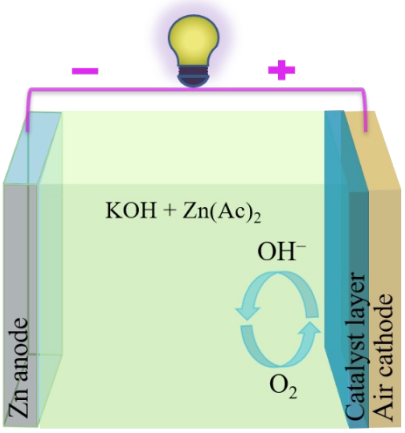

Fig. S21 Schematic illustration of the rechargeable Zn-air battery.

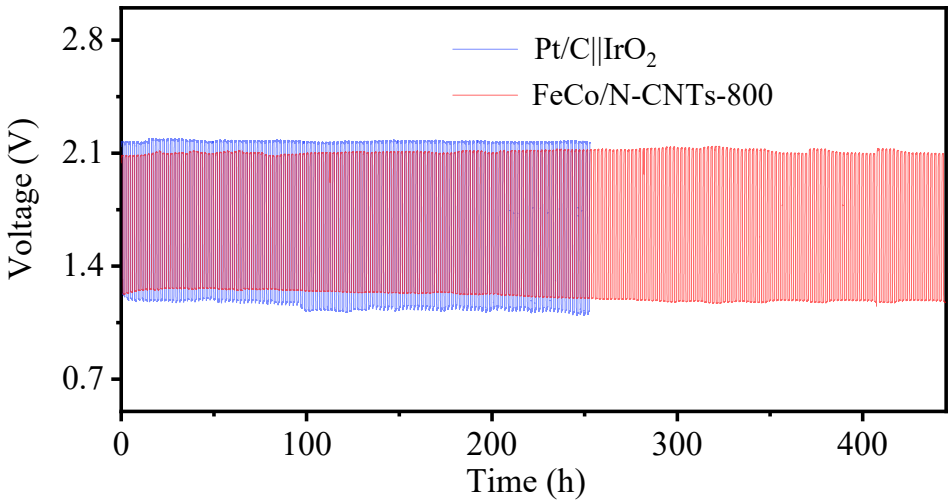

Fig. S22 Long-term cycling performance at a current density of 10 mA cm^{-2} with Pt/C||RuO_2 and FeCo/N-CNTs-800 as the air cathodes.

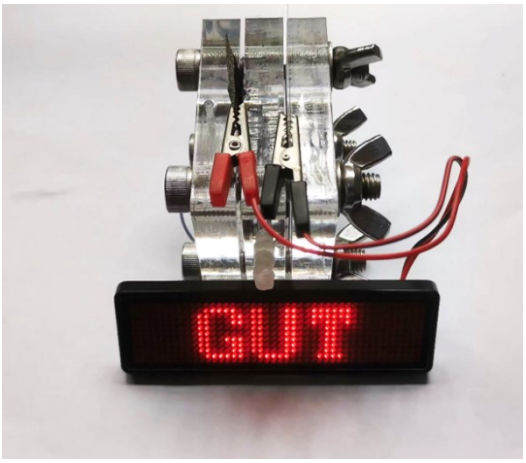

Fig. S23 Optical picture of a red LED screen powered by a ZAB assembled with FeCo/N-CNTs-800.

Table S1. XPS analysis of C 1s, N 1s, Fe 2p, and Co2p in FeCo/N-CNTs-800.

Elements	Atomic ration	Binding energy	Assignment
C 1s	86.70	284.0	C=C
		284.8	C−C
		286.0	C−N/C−O
		288.4	O−C=O
N 1s	9.05	398.7	Pyridinic-N
		400.2	Pyrrolic-N
		401.3	Graphitic-N
		404.1	Oxidized-N
Fe 2p	1.68	707.5	Fe^0
		721.1	
		711.9	Ionic state
		725.1	
		715.6	Sat
		732.6	
Co 2p	1.57	779.1	Co^0
		793.9	
		781.6	Ionic state
		796.5	
		786.9	Sat
		801.7	

Table S2. Comparison of OER/ORR electrocatalytic properties of FeCo/N-CNTs-800 with recently reported advanced catalysts.

Catalysts	OER	ORR		Reference
	$E_{J=10}$ (mV)	E_{onset}	$E_{1/2}$	
NPC/FeCo@NCNT	339	0.87	0.835	[1]
Fe_1Co_2-NC	356	1.04	0.88	[2]
FeCo/D-DNC	390	0.89	0.81	[3]
FeCo/N-GCT	500	0.91	0.79	[4]
N-GCNT/ FeCo-3	500	1.03	0.92	[5]
meso/micro-FeCo-Nx-CN	480	0.945	0.886	[6]
FeCo/Co_2P@NPCF	330	0.85	0.79	[7]
FeCo/N-CNTs@CC	408	0.87	0.816	[8]
FeCo@NCNS	367	0.98	0.827	[9]
f-FeCo-CNT	480	/	0.86	[10]
$Co_{0.5}Fe_{0.5}S$@N-MC	410	0.91	0.81	[11]
FeCo-DHO/NCNTs	320	0.91	0.80	[12]
Fe_{SA}/FeO_{NC}/NSC	/	0.99	0.86	[13]
FeCo/N-CNTs-800	**359**	**1.004**	**0.891**	**This work**

Table S3. Comparison of FeCo/N-CNTs-800 and other reported electrocatalysts for rechargeable zinc-air batteries.

Catalysts	Power density ($mW\ cm^{-2}$)	Cycling condition	Stability (h)	Reference
FeCo@MNC	115	10 min per cycle	24	[14]
NiFe@N-CF	102	20 min per cycle	100	[15]
Pd/FeCo	117	30 min per cycle	200	[16]
FeCo/N-CNTs@CC	132	10 min per cycle	40	[8]
FeCo/Co_2P@NPCF	154	10 min per cycle	107	[7]
N-GCNT/FeCo-3	97.6	10 min per cycle	40	[5]
CoNi@NCNT/NF	127	30 min per cycle	45	[17]
NiFe@N-CFs	102	60 min per cycle	150	[18]
CoNi/BCF	155	30 min per cycle	200	[19]
Ni_3Fe/N–C	134	60 min per cycle	300	[20]
FeCo/N-CNTs-800	**200.4**	**60 min per cycle**	**445**	This work

References:

1. X. Hao, Z. Jiang, B. Zhang, X. Tian, C. Song, L. Wang, T. Maiyalagan, X. Hao, Z.-J. Jiang, *Adv. Sci.,* 2021, **8**, 2004572.
2. Y. Lei, R.X. Huang, H.M. Xie, D.D. Zhang, X.Y. Liu, Y.J. Si, N. Li, *J. Alloys Compd.,* 2021, **853**, 157070.
3. G. Fu, Y. Liu, Y. Chen, Y. Tang, J.B. Goodenough, J-M. Lee, *Nanoscale*., 2018, **10**, 19937-19944.
4. X. Liu, L. Wang, P. Yu, C. Tian, F. Sun, J. Ma, W. Li, H. Fu, *Angew. Chem. Int. Ed*., 2018, **130**, 16398-16402.
5. C-Y. Su, H. Cheng, W. Li, Z-Q. Liu, N. Li, Z.F. Hou, F-Q. Bai, H-X. Zhang, T-Y. Ma, *Adv. Energy Mater*., 2017, **7**, 1602420.
6. S. Li, C. Cheng, X. Zhao, J. Schmidt, A. Thomas, *Angew. Chem. Int. Ed*., 2018, **57**, 1856-1862.
7. Q. Shi, Q. Liu, Y. Ma, Z. Fang, Z. Liang, G. Shao, B. Tang, W.Y. Yang, L. Qin, X.S. Fang, *Adv. Energy Mater*., 2020, **10**, 1903854.
8. Z. Li, H. Yang, H. Sun, S. Liang, G. Lu, Z. Liu, S. Kou, Acs. *Sustain. Chem. Eng*., 2021, **9**, 4498-4508.
9. T. Liu, S. Cai, Z. Gao, S. Liu, H. Li, L. Chen, M. Li, H. Guo, *Acta*, 2020, **335**, 135647.
10. Y. Wang, A. Kumar, M. Ma, Y. Jia, Y. Wang, Y. Zhang, G. Zhang, X. Sun, Z. Yan, *Nano Res*., 2020, **13**, 1090-1099.
11. C.L. Li, M.C. Wu, R. Liu, *Appl. Catal. B Environ*., 2019, **244**, 150e158.
12. Y. Niu, X. Teng, S. Gong, Z. Chen, *J. Mater. Chem. A*, 2020, **8**, 13725-13734.
13. F. Pan, Z. Li, Z. Yang, Q. Ma, M. Wang, H. Wang, M. Olszta, G. Wang, Z. Feng, Y. Du, Y. Yang, *Adv. Energy Mater*., 2021, **11**, 2002204.
14. W. Niu, S. Pakhira, K. Marcus, Z. Li, J. L. *Adv. Energy Mater*., 2018, **8**, 1800480.
15. Y.L. Niu, X. Teng, S.Q. Gong, Z.F. Chen, *J. Mater. Chem. A*, 2020, **8**, 13725–13734.
16. J.Y. Chen, H. Li, C. Fan, Q. W. Meng, Y.W. Tang, X.Y. Qiu, G.T. Fu, T.Y. Ma,

Adv. Mater., 2020, **32**, 2003134.

17. H. Gong, X. Zheng, K. Zeng, B. Yang, X. Liang, L. Li, Y. Tao, R. Yang, *Carbon*, 2021, **174**, 475-483.
18. Y. Wang, M. Qiao, X. Mamat, *Chem. Eng. J.*, 2020, **402**, 126214.
19. W.J. Wan, X.J. Liu, H.Y. Li, X.Y. Peng, D.S. Xi, J. Luo, *Appl. Catal. B: Environ*, 2019, **240**, 193–200.
20. Y. Wang, M. Qiao, X. Mamat, *Chem. Eng. J.*, 2020, 402, 126214.